Long-term analysis of surface temperature trends and dynamics deglaciation of the Eidembreen glacier (Svalbard) based on Landsat data for 1984–2025

Oleksiy Davydov[1,2], Yuliia Shevchuk[1]
[1] Laboratory of Geoenvironmental Research, Nature Research Centre, Vilnius, Lithuania - oleksiy.davydov@gamtc.lt, julija.shevchuk@gamtc.lt
[2] Department of Geography and Ecology, Kherson State University, Kherson, Ukraine

Keywords: Svalbard, Eidembreen, glacier, deglaciation, remote sensing

Abstract

Climate warming in the Arctic leads to accelerated glacier retreat and the formation of extensive deglaciated surfaces, substantially altering glacier–periglacial interactions. On the western coast of Svalbard, retreat of the polythermal Eidembreen Glacier is accompanied by the development of a mosaic deglaciated surface including a glacial–accumulative plain, a lagoonal basin, and a barrier spit. The aim of this study is to assess the role of the thermal regime of the deglaciated surface in glacier dynamics over a multi-decadal timescale. The analysis is based on Landsat Level-2 satellite data (Landsat 5 TM, 7 ETM+, 8 OLI/TIRS, and 9 OLI-2/TIRS-2) acquired during the period of maximum ablation (July–September) for 1984–2025. Land surface temperature (LST) and the Normalized Difference Snow Index (NDSI) were used to characterize thermal and cryospheric conditions. The satellite analysis was complemented by glacier front mapping, estimation of deglaciated area extent, and assessment of lagoon dynamics using historical aerial photographs and modern orthophotos. The results indicate an almost monotonic increase in deglaciated area from ~13.5 km² in the late 1970s to ~29.5 km² by 2025, despite pronounced interannual LST variability. Glacier retreat rates range from 19 to 42 m yr^{-1}, with maximum values in the early 21st century and renewed intensification after 2015. A strong negative correlation ($r = -0.97$) was identified between NDSI and deglaciated area, whereas LST primarily controls short-term melt intensity. These findings highlight the cumulative and inertial nature of deglaciation and emphasize the role of periglacial surface thermal properties in polythermal glacier dynamics.

1. Introduction

Global climate change is a key driver of transformations in natural processes on Earth (IPCC, 2023; WMO, 2024). Its consequences are most pronounced in the Arctic, a region characterized by high sensitivity of natural systems to climatic variability. Here, intensive deglaciation is observed, accompanied by glacier retreat and the formation of new ice-free land surfaces (Hugonnet et al., 2021; Nuth et al., 2013).

Within the Svalbard archipelago, on the western part of Spitsbergen Island in the Eidembukta Bay area, glacier retreat has led to the formation of a highly heterogeneous glacial–accumulative plain. A lagoon is located in the central part of this plain and is separated from the bay by a barrier spit. The pronounced spatial heterogeneity of the plain exerts a significant influence on the retreat dynamics of adjacent glaciers, including the Eidembreen Glacier.

The Eidembreen Glacier is classified as polythermal (Kotlyakov, 1984; Paterson, 1994), which results in pronounced spatial heterogeneity of its dynamics along the glacier margin. When analysing the dynamics of polythermal glaciers, not only air temperature but also the total amount of heat accumulated within the adjacent periglacial surface is of key importance.

In the Eidembreen Glacier area, the main deglaciation processes develop during a relatively short time interval, from July to September. Under these conditions, high glacier retreat rates may be associated with the accumulation of a certain amount of heat on the adjacent surfaces. The character of the underlying surface plays a significant role, including the presence of land areas with specific relief as well as water bodies of varying depth and with different water-exchange regimes. The combined influence of these factors determines the surface heat balance and, consequently, the rates of deglaciation.

Accordingly, the aim of this study is to investigate the relationship between the dynamic trends of the Eidembreen Glacier and the characteristics of the thermal regime of the periglacial surface as one of the key factors controlling the deglaciation of polythermal glaciers.

To achieve this aim, the following objectives were formulated:

1. To reconstruct the spatio-temporal dynamics of the Eidembreen Glacier front retreat over the period 1938–2025 based on archival aerial photographs and satellite data.

2. To investigate changes in snow and ice cover using the NDSI and to assess its role as an indicator of long-term deglaciation processes.

3. To analyse the spatial distribution and long-term dynamics of land surface temperature (LST) across glacial, aquatic, and deglaciated surfaces during the warm season.

4. To perform a correlation analysis between overall glacier retreat dynamics and the NDSI and LST indices in order to identify general deglaciation conditions and assess its spatial selectivity.

2. Study Area

The study area is located on West Spitsbergen Island within the Svalbard archipelago (Fig. 1A), in the southwestern part of Oscar II Land, along the coast of Eidembukta Bay. In genetic terms, the study area represents a periglacial surface (Fig. 1B) that has formed as a result of the retreat of the Eidembreen Glacier over the last ~100 years.

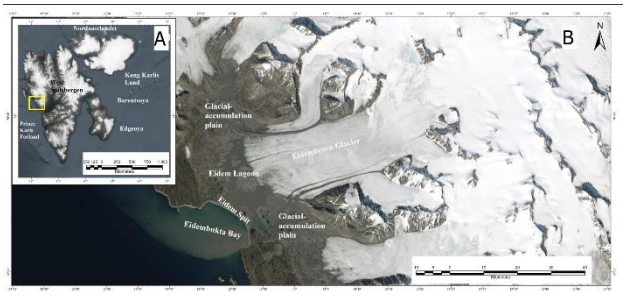

Figure 1. Geographical location and main natural features of the study area: A — location of the study area within the Svalbard archipelago; B — general view and morphological characteristics of the study area.

In the first half of the 20th century, the studied periglacial surface was almost entirely covered by the body of the Eidembreen Glacier (Fig. 2). Prolonged glacier retreat played a key role in shaping the structure and composition of this surface.

Figure 2. General view of the study area in 1938 (aerial photograph from the TopoSvalbard resource, Norwegian Polar Institute).

In plan view, the studied surface has a fan-shaped configuration, expanding from the southeastern part toward the west and northwest. The minimum width of the surface, approximately 2.0 km, is recorded in its southeastern sector. In the southern and southwestern sectors, the width increases to 2.91 km, reaching a maximum of 3.23 km in the western part, and then decreases to 2.62 km in the northwestern sector. As of 2025, the total area of the studied periglacial surface is approximately 29.5 km².

The western coast of Spitsbergen is characterized by an Arctic maritime climate, moderated by the influence of the warm West Spitsbergen Current (Loeng, 1991; Årthun et al., 2012; Muckenhuber et al., 2016). Mean annual air temperatures range from −4 to −6 °C, decreasing to −12…−16 °C in January and increasing to +3…+6 °C in July (Hanssen-Bauer et al., 2019). Mean annual precipitation varies between 400 and 800 mm, with a substantial proportion falling as snow (Humlum, 2002; Førland et al., 2011).

Under these climatic conditions, a wide variety of glacier types are widespread across the Svalbard archipelago (Bamber, 1989; Nuth et al., 2013). The Eidembreen Glacier (central coordinates: 78°23′4.71″ N; 12°57′13.43″ E) represents one of the key relief-forming factors within the studied periglacial surface. It is a valley glacier approximately 18 km in length, which currently discharges into the Eidem Lagoon area (Bamber, 1989; Mangerud & Landvik, 2007).

The accumulation area of the glacier is located at elevations of approximately 580 m a.s.l. within the Trollheimen mountain region (Bamber, 1989; Mangerud & Landvik, 2007). The glacier exhibits a dendritic structure: tributary glaciers Heksebreen and Stallobreen join it from the southeast, while Huldrebreen and Austgøtabreen enter from the northeast (Myhre, 1988). The glacier is classified as polythermal and is characterized by active melting processes occurring both at the surface and within the subglacial zone (Kotlyakov, 1984; Tretiakov et al., 2021).

The periglacial surface adjacent to the glacier is characterized by a complex morphological structure (Davydov et al., 2025). The following main morphological elements can be distinguished within it: a glacio-accumulative plain, the Eidem Lagoon basin, and the Eidem barrier spit separating the lagoon from the waters of Eidembukta Bay (Fig. 1B).

The glacio-accumulative plain is the main morphogenetic element of the study area and is characterized by the largest spatial extent and the highest absolute elevations. It exhibits pronounced morphological complexity and surface mosaicity, reflecting repeated shifts between glacial and glaciofluvial conditions during deglaciation (Davydov et al., 2025). The morphological structure of the plain is formed by a combination of landforms of glacial, glaciofluvial, glaciolacustrine, and coastal genesis.

The predominance of landforms and deposits of glacial origin indicates the dominant role of glacial accumulation and erosion in shaping the study area. At the same time, the well-developed network of drainage channels, glaciofluvial valleys, and outwash fans reflects a high intensity of moraine material reworking by meltwater. Marginal moraine ridges record the positions of the glacier front at individual stages of its retreat, while the presence of glaciolacustrine plains indicates episodic meltwater accumulation and the formation of temporary water bodies.

The Eidem Lagoon is located in the central part of the study area (central coordinates: 78°22.505′ N; 12°50.936′ E) and is characterized by a complex and dynamic configuration. As of 2025, seven expanded water basins connected by narrow straits are distinguished within the lagoon (Fig. 1B) (Davydov et al., 2025). Over recent decades, a persistent increase in lagoon area has been observed, from 3.2 km² in 1993 to 6.6 km² in 2023 (Šiaulys et al., 2025).

The study area and the Eidem Lagoon are separated from the Eidembukta Bay by the Eidem barrier spit (Fig. 1B). The spit is approximately 3.4 km long; its width varies from 60–200 m in constricted sections to 350–500 m in widened parts, while surface elevations range between 1.4 and 3.6 m a.s.l. The spit has a concave arcuate shape with a curvature radius of about 2.27 km and extends from the northwestern point (78°22.238′ N; 12°45.757′ E) toward the southeast (78°21.230′ N; 12°52.511′ E). In the distal part of the spit, a shallow strait with depths of up to 1.5 m facilitates water exchange between the lagoon and the bay.

3. Materials and Methods

The materials of this study are based on remote sensing data of the periglacial surface of western Spitsbergen Island (Svalbard

Archipelago) in the Eidembukta Bay area, acquired and processed by the staff of the Nature Research Centre (Vilnius, Republic of Lithuania).

Landsat Level-2 satellite data, providing radiometric and atmospheric correction and suitable for long-term monitoring, were used in this study. The analysis was based on data from the following sensors: Landsat 5 TM (1984–2011), Landsat 7 ETM+ (1999–2021), Landsat 8 OLI/TIRS (2013–2021), and Landsat 9 OLI-2/TIRS-2 (2021–2025).

To ensure the comparability of the results, satellite images acquired during the period of maximum ablation (July–September) for 1984–2025 were used, with minimal cloud cover over the study area. The spatial resolution of the optical bands was 30 m; the thermal bands were resampled to the same spatial resolution.

3.1. Data processing and cartographic analysis

Pre-processing of satellite data, spatial analysis, and cartographic visualization were performed in the GIS environment ArcGIS Pro. The processing workflow included georeferencing, clipping to the study area boundaries, calculation of thermal and spectral indices, surface classification, and vectorization of the glacier front and deglaciated areas.

The construction of time series, statistical analysis, and visualization of the results were carried out in RStudio using the packages *terra*, *sf*, *dplyr*, *tidyr*, *lubridate*, and *ggplot2* (R Core Team, 2019).

3.2. Calculation of Land Surface Temperature (LST)

Land Surface Temperature (LST) was calculated using the thermal infrared bands of Landsat Level-2 data. The methodology included the conversion of spectral radiance to brightness temperature, correction for surface emissivity, and subsequent conversion of temperature values from Kelvin to degrees Celsius according to the following equation:

$$LST_{(°C)} = LST_{(K)} - 273{,}15 \qquad (1)$$

The resulting LST rasters were used to analyze the spatial distribution of the thermal regime of glacial, aquatic, and deglaciated surfaces during the warm season (Li et al., 2013; Roy & Bari, 2022).

3.3. Calculation of the Snow and Ice Cover Index (NDSI)

To identify snow and ice cover, the Normalized Difference Snow Index (NDSI) was applied (Shuman et al., 2014; Mohammadi et al., 2023), calculated using the following formula:

$$NDSI = \frac{Green - SWIR}{Green + SWIR} \qquad (2)$$

where Green denotes the green spectral band (Band 3 for Landsat TM, ETM+, and OLI), and SWIR represents the shortwave infrared band (Band 6 for Landsat TM, Band 5 for ETM+, and Band 6 for Landsat OLI).

A threshold value of NDSI > 0.4 was applied to delineate stable snow and ice cover. The accuracy of the classification results was visually validated using false-color composites of the satellite imagery (Shangguan et al., 2006; Yan et al., 2021).

3.4. Zones of Active Melting and Deglaciation Dynamics

Zones of active melting were delineated based on the logical intersection of the conditions LST > 0 °C and NDSI > 0.4, allowing the identification of areas where snow and ice cover persists under positive surface temperatures, thereby indicating zones of active surface melting (Duan et al., 2021).

Mapping of deglaciated surfaces and digitization of the glacier front were performed for individual time slices. Based on the resulting vector datasets, areas of deglaciated surfaces and glacier retreat rates were calculated for individual sectors (Carrivick & Heckmann, 2017; Hall et al., 1995).

To extend the temporal coverage of the analysis, archival aerial photographs from 1938 (TopoSvalbard resource) as well as orthophotos acquired during field surveys in 2022 were additionally used.

3.5. Statistical Analysis

Statistical analyses were performed in RStudio using descriptive statistics and correlation analysis. Pearson correlation coefficients were calculated to assess relationships between:

– the area of the deglaciated surface and lagoon size;

– NDSI values and the area of ice-free surfaces;

– land surface temperature (LST) and short-term glacier retreat dynamics.

The combined use of thermal (LST) and spectral (NDSI) indicators enabled a quantitative assessment of the role of surface thermal conditions and morphostructural characteristics in controlling deglaciation processes.

4. Results

4.1. Dynamics of the Eidembreen Glacier Retreat (1938–2025)

The starting point for the analysis of the Eidembreen Glacier retreat dynamics was the 1936–1938 period, when the Norwegian Polar Institute conducted aerial photographic surveys of the Svalbard archipelago (Norwegian Polar Institute, 1936–1938). Based on the analysis of archival aerial photographs, the position of the glacier frontal margin was reconstructed, providing insight into the morphological conditions of the study area at the initial stage of investigation.

The geographical coordinates of key points along the outer boundary of the glacier, refined using the TopoSvalbard resource, were adopted as the reference state for subsequent spatio-temporal analysis of deglaciation.

During the period of aerial photography, almost the entire study area was covered by the body of the Eidembreen Glacier, whose frontal margin partially extended directly into the waters of Eidembukta Bay. Ice-free areas were preserved only within the zone of convergence with the Geografbreen and Vestgötabreen glaciers, as well as in the southwestern part of the study area, where two proglacial lakes already existed and the body of the Eidem barrier spit had formed (Fig. 2).

Comparison of the glacier front position during the period of aerial photography with its position derived from satellite data

for 1978 made it possible to determine the parameters of the deglaciated surface and to calculate mean glacier retreat rates over a 40-year interval. During this period, mean retreat rates ranged from 27 to 33 m yr^{-1}, except for the southern part of the study area (sector d in Fig. 3), where they did not exceed 20 m yr^{-1} (Fig. 3). By 1978, the total area of the deglaciated surface had reached approximately 13.5 km², of which 2.3 km² was occupied by the lagoon, predominantly located within the southern sector of the study area.

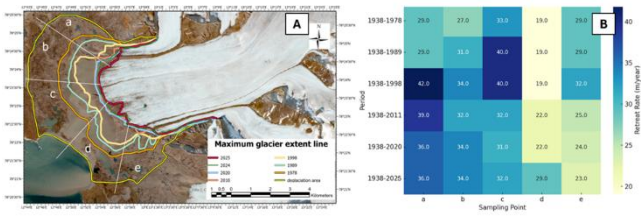

Figure 3. Results of the spatio-temporal and quantitative analysis of long-term trends in the retreat of the Eidembreen Glacier during 1938–2025: A — long-term changes in the position of the glacier frontal margin within five sectors; B — quantitative estimates of glacier frontal retreat rates over the long-term period within five sectors.

During the 1980s, a pronounced spatial differentiation in glacier retreat rates began to emerge. The highest values (31–40 m yr^{-1}) were recorded in the western (b) and southwestern (c) parts of the deglaciated surface, whereas retreat rates of approximately 30 m yr^{-1} were observed in the southeastern (e) and northwestern (a) sectors. The lowest retreat rates (up to 20 m yr^{-1}) were consistently recorded in the southern sector (d), which is predominantly represented by the lagoon water area (Fig. 3).

During the 1990s, the highest glacier retreat rates were recorded, accompanied by pronounced spatial differentiation. Within the western (b), southwestern (c), and southeastern (e) sectors of the deglaciated surface, retreat rates ranged from 32 to 40 m yr^{-1}. In the northwestern sector (a), retreat rates exceeded 40 m yr^{-1}, whereas in the southern sector (d) they decreased to approximately 20 m yr^{-1} (Fig. 3).

During the 2000s, deglaciation rates slightly decreased. In the western (b) and southwestern (c) sectors, glacier retreat rates were approximately 32 m yr^{-1}, whereas in the southern (d) and southeastern (e) sectors they ranged between 22 and 25 m yr^{-1}. In the northwestern sector (a), retreat rates remained relatively high, reaching approximately 39 m yr^{-1} (Fig. 3).

During the subsequent decade, no substantial changes in deglaciation rates or in the pattern of their spatial differentiation were observed. In the northwestern sector (a), glacier retreat rates were approximately 36 m yr^{-1}, in the western (b) and southwestern (c) sectors they ranged between 31 and 34 m yr^{-1}, whereas in the southern (d) and southeastern (e) sectors they varied from 22 to 24 m yr^{-1} (Fig. 3).

During the 2020–2025 period, glacier retreat rates generally remained stable, with a localized increase observed in the southern sector (d) (Fig. 3). By 2025, the total area of the deglaciated surface had increased to 29.5 km².

The analysis of the relationship between the areas of deglaciated land surfaces and the lagoon revealed their synchronous increase throughout the entire observation period. The lagoon area expanded from approximately 2.3 km² in the late 1970s to about 6.8 km² by 2025. Statistical analysis showed a very strong correlation between the area of the deglaciated surface and lagoon size ($r = 0.968$), indicating a close linkage between glacier retreat and the formation of periglacial water bodies.

4.2. Dynamics of Snow and Ice Cover (1985–2025)

The long-term dynamics of snow and ice cover within the study area were assessed using the Normalized Difference Snow Index (NDSI). Analysis of the spatial distribution of NDSI values indicates a persistent reduction in the extent of snow and ice cover throughout the entire observation period. The generated NDSI maps (Fig. 4) demonstrate a clear distinction between areas with stable snow and ice cover (NDSI > 0.4) and deglaciated surfaces characterized by low or negative index values.

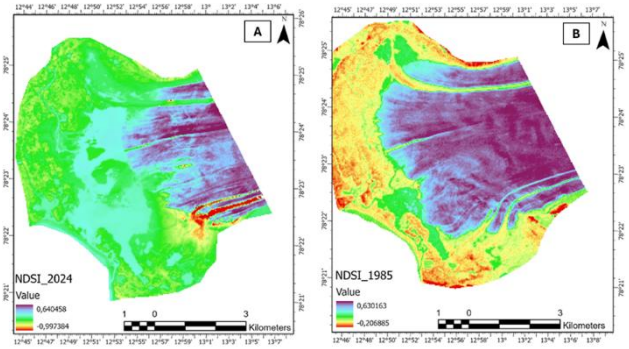

Figure 4. Spatial distribution of the Normalized Difference Snow Index (NDSI) derived from: A — Landsat 9 OLI-2/TIRS-2 (August 2024); B —.Landsat 5 TM (August 1985) Values > 0.4 indicate stable snow cover, values between 0 and 0.4 represent patchy or contaminated snow, and values < 0 correspond to snow-free surfaces.

During the 1980s, NDSI values across most of the study area exceeded 0.4, indicating the dominance of stable snow and ice cover. By 2025, the proportion of such areas had decreased substantially. The highest NDSI values are associated with the central part of the glacier body and shaded areas of the surrounding mountain terrain, whereas the lowest values are characteristic of deglaciated surfaces represented by glaciofluvial plains and lagoon water bodies. Within the deglaciated surface, NDSI values exhibit a fragmented spatial pattern, indicating the absence of a stable snow cover and the predominance of seasonal snow remnants.

4.3. Dynamics of Glacier and Deglaciated Surface Temperature (LST)

The spatial distribution of land surface temperature (LST) derived from Landsat data shows a clear differentiation between glacier, water, and deglaciated surfaces. The lowest LST values are consistently observed over the glacier surface and snow-covered areas. Intermediate values are characteristic of lagoon water bodies, whereas the highest LST values are associated with exposed land surfaces within the deglaciated areas (Fig. 5).

The analysis of land surface temperature was conducted for the warm season (July–September). Over the long-term period, LST values on the glacier surface fluctuated around 0 °C, with predominantly negative temperatures (−2 to −4 °C) and episodic increases to +4 to +6 °C, which are associated with the presence of surface debris (supraglacial moraine).

Within lagoon water bodies, LST values exhibit relative stability and range between +2 and +6 °C, with lower temperatures observed in areas proximal to the glacier and higher values recorded in more distant and shallow zones.

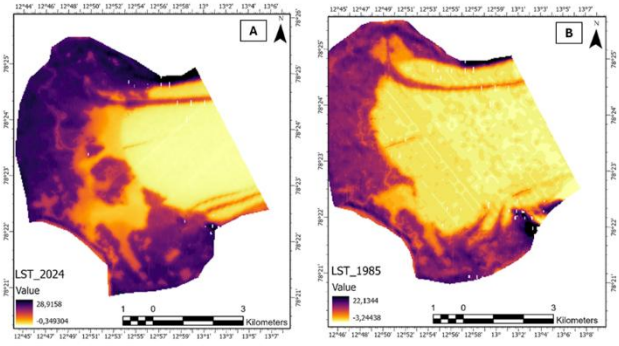

Figure 5. Spatial distribution of Land Surface Temperature (LST) derived from: A — Landsat 9 OLI-2/TIRS-2 (August 2024); B —. Landsat 5 TM (August 1985).

Land surfaces within the deglaciated area are characterized by the highest thermal contrast, with LST values ranging from +1 to +20 °C, depending on surface position and the intensity of solar radiation. The long-term dynamics of mean LST values indicate a gradual increase in surface temperatures during 1985–2000, followed by a phase of relative stabilization in 2000–2015, and a renewed increase in LST over the last decade, reaching maximum values in the most recent period (Fig. 5).

4.4. Correlation Results and Identification of Active Melting Zones

A combined correlation analysis of glacier retreat dynamics, land surface temperature (LST), and the snow and ice cover index (NDSI) enabled the identification of zones of active deglaciation characterized by the simultaneous fulfillment of the conditions LST > 0 °C and NDSI > 0.4. These zones are predominantly localized along the glacier margins and in areas subjected to maximum solar insolation.

From a temporal perspective, zones of active melting are most pronounced during periods of elevated LST values, particularly in the late 20th century and after 2015, indicating an intensification of deglaciation processes under changing climatic conditions. The long-term dynamics of LST, NDSI, and the area of the deglaciated surface exhibit coordinated but oppositely directed trends over the 1985–2025 period (Fig. 6).

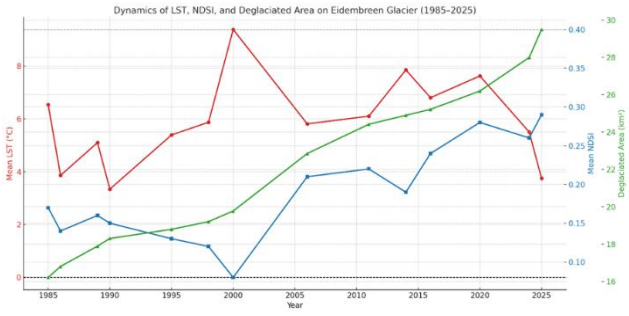

Figure 6. Temporal dynamics of mean Land Surface Temperature (LST), snow and ice cover index (NDSI), and the area of the deglaciated surface of the Eidembreen Glacier over the 1985–2025 period. The red line represents mean LST (°C), the blue line indicates mean NDSI, and the green line denotes the area of the deglaciated surface (km²).

Overall, the results indicate a persistent and continuous retreat of the Eidembreen Glacier over an observation period of nearly 90 years. Despite a moderate slowdown in deglaciation rates during the 21st century, glacier retreat rates remain high. A clear pattern is observed whereby retreat rates are higher in sectors of the deglaciated surface dominated by land areas compared to zones represented by water bodies.

The obtained results indicate that the deglaciation of the Eidembreen Glacier during the 1938–2025 period exhibits a directional, persistent, inertial, and cumulative character. Despite the presence of interdecadal fluctuations in glacier retreat rates, the overall trend of expansion of the deglaciated surface has been maintained throughout the entire observation period, indicating the dominance of long-term controlling processes over short-term climatic variability.

The spatial differentiation of deglaciation rates within the glacier frontal zone is closely related to the type of underlying surface. In sectors of the deglaciated area dominated by land surfaces, glacier retreat rates are consistently higher than in zones represented by water bodies. This pattern reflects the buffering effect of the aquatic environment, which is associated with its high heat capacity and reduced amplitudes of diurnal and seasonal temperature fluctuations, thereby limiting the intensity of surface melting.

The combined analysis of land surface temperature (LST) and the snow and ice cover index (NDSI) revealed their distinct roles in deglaciation processes. An increase in LST values in the late 20th century was accompanied by an acceleration of glacier retreat, indicating the role of surface temperature as a trigger for intensified melting. However, subsequent LST fluctuations (periods of decrease, stabilization, and renewed increases) did not lead to changes in the overall deglaciation trend, emphasizing the inertial nature of the glacier system. In this case, deglaciation is governed not so much by short-term thermal conditions as by the accumulated multi-decadal heat balance and the morphostructural characteristics of the glacier and its adjacent periglacial zone.

In contrast to LST, the Normalized Difference Snow Index (NDSI) exhibits a strong and stable negative correlation with the area of the deglaciated surface ($r = -0.97$), reflecting the long-term degradation of snow and ice cover. The consistent decline in mean NDSI values from the late 1980s to 2025 records the progressive reduction of stable snow cover and its replacement by exposed terrestrial and aquatic surfaces. Thus, NDSI serves as a reliable indicator of the cumulative effect of deglaciation, whereas LST primarily reflects short-term thermal responses of the surface.

A comparison between deglaciation dynamics and climatic parameters shows that the increase in the area of the deglaciated surface is accompanied by a decrease in atmospheric precipitation (Fig. 7). This result indicates the multifactorial nature of glacier retreat, in which deglaciation is governed not by a single climatic parameter but by the combined influence of several interacting factors.

In the study area, the thermal regime of the periglacial surface, its morphological structure, and the decline in precipitation jointly create conditions that promote sustained and directed glacier retreat. Reduced precipitation limits snow accumulation

in the accumulation zone, whereas the increased heat capacity and thermal inertia of the deglaciated surface enhance ablation processes, thereby maintaining the overall deglaciation trend.

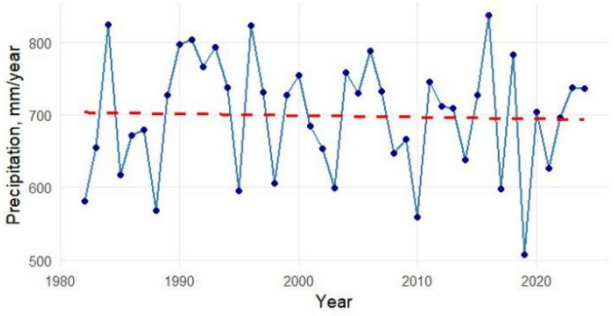

Figure 7. Long-term dynamics of atmospheric precipitation in the Western Spitsbergen region (based on data from the NASA POWER database, NASA).

Under the conditions of western Svalbard, glacier deglaciation is controlled not only by atmospheric warming and a decline in precipitation, but also by the thermal properties of the newly forming deglaciated surface. The expansion of exposed land areas leads to a reduction in surface albedo and enhanced absorption of solar radiation, establishing a positive feedback mechanism that promotes further acceleration of glacier melt.

5. Conclusions

Based on the obtained results, the following conclusions were drawn:

1. Based on archival aerial photographs and satellite data, the spatiotemporal dynamics of the Eidembreen Glacier front retreat were reconstructed for the period 1938–2025. The results indicate that deglaciation is characterized by a persistent, inertial, and cumulative pattern, manifested in continuous glacier retreat at mean rates of 19–42 m yr^{-1} and an expansion of the deglaciated area from approximately 13.5 to 29.5 km^2.

2. Analysis of the snow and ice cover using the Normalized Difference Snow Index (NDSI) revealed a persistent reduction in the extent of snow- and ice-covered surfaces during 1985–2025. The consistent decrease in mean NDSI values reflects the long-term degradation of the snow–ice cover and confirms its reliability as an indicator of the cumulative effects of deglaciation.

3. Spatial analysis of land surface temperature (LST) revealed pronounced thermal differentiation between glacial, aquatic, and deglaciated surfaces. Maximum LST values are characteristic of terrestrial areas within the deglaciated surface, whereas minimum values are associated with the glacier body. This pattern highlights the key role of the underlying surface type in shaping the thermal regime of the periglacial zone. On a multi-decadal timescale, an increasing trend in LST values is observed across the study area.

4. Correlation analysis between glacier retreat dynamics and the NDSI and LST indices showed that land surface temperature (LST) acts as a trigger for short-term intensification of melting processes, whereas NDSI reflects long-term deglaciation trends. A pronounced spatial selectivity of deglaciation was identified: glacier retreat rates are higher in areas dominated by terrestrial surfaces than in zones represented by water bodies. This pattern is controlled by differences in the thermal balance and heat capacity of the underlying surface.

References

Årthun, M., Eldevik, T., Smedsrud, L.H., Skagseth, Ø., Ingvaldsen, R.B., 2012: Quantifying the influence of Atlantic heat on Barents Sea ice variability and retreat. *Journal of Climate*, 25(13), 4736–4743. doi:10.1175/JCLI-D-11-00466.1.

Bamber, J.L., 1989: Ice/bed interface and englacial properties of Svalbard ice masses deduced from airborne radio-echosounding data. *Journal of Glaciology*, 35 (119), 30–37. doi:10.3189/002214389793701392.

Carrivick, J.L., Heckmann, T., 2017: Short-term geomorphological evolution of proglacial systems. *Earth Surface Processes and Landforms*, 42 (15), 2561–2579. doi:10.1002/esp.4178.

Davydov, O., Damušytė, A., Bitinas, A., 2025: Geological structure features of the Eidembukta (Eidem Lagoon) area (Svalbard Archipelago). In: *Sea and Coastal Research 2024*. Conference materials. Klaipėda University, Klaipėda, 24–25. (in Lithuanian).

Duan, S.-B., Li, Z.-L., Wang, C., Zhang, S., Tang, B.-H., Leng, P., Gao, M.-F., 2021: Validation of Landsat land surface temperature product in the conterminous United States using in situ measurements from SURFRAD, ARM, and NDBC sites. *International Journal of Digital Earth*, 14, 640–660. doi:10.1080/17538947.2020.1862319.

Førland, E.J., Benestad, R.E., Hanssen-Bauer, I., Haugen, J.E., Skaugen, T.E., 2011: Temperature and precipitation development at Svalbard 1900–2100. *Advances in Meteorology*, 2011, 893790. doi:10.1155/2011/893790.

Hall, D.K., Riggs, G.A., Salomonson, V.V., 1995: Development of methods for mapping global snow cover using moderate resolution imaging spectroradiometer data. *Remote Sensing of Environment*, 54 (2), 127–140. doi:10.1016/0034-4257(95)00137-P.

Hanssen-Bauer, I., Førland, E.J., Hisdal, H., Mayer, S., Sandø, A.B., Sorteberg, A., 2019: *Climate in Svalbard 2100 – a knowledge base for climate adaptation*. NCCS Report 1/2019. Norwegian Centre for Climate Services, Norway.

Hugonnet, R., McNabb, R., Berthier, E., Menounos, B., Nuth, C., Girod, L., Farinotti, D., Huss, M., Dussaillant, I., Brun, F., Kääb, A., 2021: Accelerated global glacier mass loss in the early twenty-first century. *Nature*, 592 (7856), 726–731. doi:10.1038/s41586-021-03436-z.

Humlum, O., 2002: Modelling late 20th-century precipitation in Nordenskiöld Land, Svalbard, by geomorphic means. *Norwegian Journal of Geography*, 56 (2), 96–103. doi:10.1080/002919502760056413.

IPCC, 2023: *Climate Change 2023: Synthesis Report*. Contribution of Working Groups I, II and III to the Sixth Assessment Report of the Intergovernmental Panel on Climate Change. IPCC, Geneva.

Kotlyakov, V.M. (Ed.), 1984: *Glatsiologicheskii slovar'*. 2nd ed. Gidrometeoizdat, Leningrad. (in Russian).

Li, Z.-L., Tang, B.-H., Wu, H., Ren, H., Yan, G., Wan, Z., Trigo, I.F., Sobrino, J.A., 2013: Satellite-derived land surface temperature: Current status and perspectives. *Remote Sensing of Environment*, 131, 14–37. doi:10.1016/j.rse.2012.12.008.

Loeng, H., 1991: Features of the physical oceanographic conditions of the Barents Sea. *Polar Research*, 10 (1), 5–18. doi:10.1111/j.1751-8369.1991.tb00630.x.

Mohammadi, B., Pilesjö, P., Duan, Z., 2023: The superiority of the adjusted normalized difference snow index (ANDSI) for mapping glaciers using Sentinel-2 multispectral satellite imagery. *GIScience & Remote Sensing*, 60 (1), 2257978. doi:10.1080/15481603.2023.2257978.

Muckenhuber, S., Nilsen, F., Korosov, A., Sandven, S., 2016: Sea ice cover in Isfjorden and Hornsund, Svalbard (2000–2014) from remote sensing data. *The Cryosphere*, 10 (1), 149–158. doi:10.5194/tc-10-149-2016.

Myhre, A.M., 1988: The Western Svalbard margin. *Marine and Petroleum Geology*, 5 (2), 143–156. doi:10.1016/0264-8172(88)90005-4.

Norwegian Polar Institute, 1936–1938: Historical aerial photographs of Svalbard. TopoSvalbard data portal.

Nuth, C., Kohler, J., König, M., von Deschwanden, A., Hagen, J.O., Kääb, A., Moholdt, G., Pettersson, R., 2013: Decadal changes from a multi-temporal glacier inventory of Svalbard. *The Cryosphere*, **7**, 1603–1621. doi:10.5194/tc-7-1603-2013.

Paterson, W.S.B., 1994: *The Physics of Glaciers*. 3rd ed. Butterworth-Heinemann, Oxford.

R Development Core Team. 2019. R Core Team (2020). R: A Language and Environment for Statistical Computing. R Foundation for Statistical Computing. Vienna, Austria. R Foundation for Statistical Computing. https://Www. R-Project.Org/.

Roy, B., Bari, E., 2022: Examining the relationship between land surface temperature and landscape features using spectral indices with Google Earth Engine. *Heliyon*, 8 (9), e10668. doi:10.1016/j.heliyon.2022.e10668.

Shangguan, D., Liu, S., Ding, Y., Ding, L., Xiong, L., Cai, D., Li, G., Lu, A., Zhang, S., Zhang, Y., 2006: Monitoring the glacier changes in the Muztag Ata and Konggur mountains, East Pamirs, based on Chinese Glacier Inventory and recent satellite imagery. *Annals of Glaciology*, 43, 79–85. doi:10.3189/172756406781812393.

Shuman, C.A., Hall, D.K., DiGirolamo, N.E., Mefford, T.K., Schnaubelt, M.J., 2014: Remote sensing of glacier surface temperatures. *Remote Sensing of Environment*, 140, 348–358. doi:10.1016/j.rse.2013.09.002.

Šiaulys, A., Šaškov, A., Kilmonaitė, G., Lukashanets, D., Politi, T., Samuilovienė, A., Zaiko, A., Olenin, S., 2025: A dataset on bathymetry and hydrology of an emerging periglacial lagoon in Svalbard, Arctic. *Data in Brief*, 59, 111304. doi:10.1016/j.dib.2025.111304.

Tretiakov, M.V., Bryzgalo, V.A., Rumiantseva, E.V., Romashova, K.V., 2021: *Freshwater resources of Western Spitsbergen in modern conditions*. Arctic and Antarctic Research Institute, St. Petersburg. (in Russian).

WMO, 2024: *State of the Global Climate 2024*. World Meteorological Organization, Geneva.

Yan, S., Xu, L., Yu, G., Yang, L., Yun, W., Zhu, D., Ye, S., Yao, X., 2021: Glacier classification from Sentinel-2 imagery using spatial-spectral attention convolutional model. *International Journal of Applied Earth Observation and Geoinformation*, 102, 102445. doi:10.1016/j.jag.2021.102445.